Solid Earth Discuss., https://doi.org/10.5194/se-2017-134
Manuscript under review for journal Solid Earth
Discussion started: 16 January 2018

Solid Earth Discussions

The effect of obliquity on temperature in subduction zones: insights from 3D numerical modeling.

Alexis Plunder[1,a], Cédric Thieulot[1], and Douwe J. J. van Hinsbergen[1]

[1]Department of Earth Sciences, Utrecht University, The Netherlands

[a]Now at Sorbonne Université, CNRS-INSU, Institut des Sciences de la Terre Paris, ISTeP UMR 7193, F-75005 Paris, France

Correspondence to: A. Plunder, (alex.plunder@gmail.com)

Abstract. In subduction zones the geotherm is thought to vary as a function of the subduction rate and the age of the subducting lithosphere. Along a single subduction zone the rate of subduction can strongly vary due to changes in the angle between the trench and the plate convergence vector, namely the subduction obliquity. We currently observe such a configuration all around the Pacific (e.g. Marianna, Chile, Aleutians). Subduction obliquity is also supposed in the geological record of Western and Central Turkey. In order to investigate this effect, we designed and computed simple thermo-kinematic finite element 3D numerical models. We prescribe the trench geometry by means of a simple mathematical function and compute the mantle flow in the mantle wedge only by solving the equation of mass and momentum conservation. We then solve the energy conservation equation until steady-state is reached. We analyse the results (i) in terms of mantle wedge flow with emphasis on the trench-parallel component and (ii) in terms of temperature along the plate interface by means of maps and depths-temperature path at the interface. We show that the effect of the trench curvature on the geotherm is substantial. A small obliquity yields a small but not negligible trench parallel mantle flow leading to differences of 50°C along strike of the model. With increasing obliquity, the trench parallel component of the velocity consequently increases and the temperature variation can be as important as 200°C along strike. This can even be larger with varying plate velocity. Finally, we discuss the implication of our simulations for the ubiquitous oblique systems that are observed on Earth, the limitation of our modeling approach and the significance for the geological record with an emphasis on the case study of Western and Central Turkey.

1 Introduction

Oceanic subduction and continental collision zones represent approximately 55 000 kilometres of converging plate boundaries on Earth today. They are widely associated with arc magmatism and seismicity, which in turn are mainly a response to the thermal structure and geotherm of a subduction zone. Numerous studies have addressed the effect of temperature in subduction zones and its link to the coupling of the subduction interface (Wada and Wang, 2009) and related seismicity (Kirby et al., 1996; Peacock and Wang, 1999; Hacker et al., 2003b), as well as the release of fluids (van Keken et al., 2011; Wada et al., 2012), and the associated generation of melt (Gorczyk et al., 2007; Bouilhol et al., 2015), mostly using 2D high resolution numerical models. Temperature distributions in subduction zones are thought to vary primarily as a function of the subduction rate and the age of the subducting lithosphere, whereby lower subduction rates and younger lithosphere tend to increase temperatures at the subduction interface (Kirby et al., 1991; Peacock and Wang, 1999; van Keken et al., 2011). The geotherm is then mainly controlled by the mantle flow in the convergence direction (i.e. poloidal flow) with presumably little variation along-strike.

Real subduction zones, however, tend to have lateral variations in trench strike, and hence subduction obliquity. In fact, some degree of oblique subduction is the rule rather than the exception, both in todays snapshot of plate tectonics (e.g. Fig. 1 and Bird (2003)) as well as in the geological past (Stampfli and Borel, 2002), e.g. in the Mediterranean region (e.g. van Hinsbergen et al., 2016; Menant et al., 2016), the South-American system (Vérard et al., 2012; Schepers et al., 2017) or the western North American margin (Johnston, 2001; Liu et al., 2008).

Lateral variations in subduction obliquity may conceptually influence the temperature at the subduction interface in two ways. First, oblique subduction adds a component of horizontal relative motion between slab and mantle wedge - toroidal flow - to the poloidal flow in the mantle wedge, which may influence heat advection. Second, higher subduction obliquity leads to a lower net subduction rate. Intuitively, this may suggest that increasing subduction obliquity may be associated with higher temperatures at the subduction interface. Investigating the effect of trench curvature on along-strike variations of temperature at the plate interface may thus help to explain along-strike variations in e.g. generation of magma, or seismicity along subduction zones, or to help the reconciliation of contrasting metamorphic records with kinematic reconstructions. Few studies were conducted on the effect of obliquity/geometry on the geotherm of subduction zone (e.g. Ji and Yoshioka, 2015) and most studies mainly focused on mantle flow patterns (Honda and Yoshida, 2005; Kneller and van Keken, 2008; Jadamec and Billen, 2010, 2012; Bengtson and Van Keken, 2012; Morishige and van Keken, 2014; Wada et al., 2015)

In this paper, we aim to study the effect of the trench curvature on along-strike temperature distribution changes in subduction zones. In particular, we aimed to test a recent hypothesis that a major, $>300°C$ along-strike contrast in subduction zone temperature concluded from the geology of Turkey resulted from a corresponding major change in trench strike (see next section; van Hinsbergen et al., 2016). To this end, a simple 3D thermo-kinematic numerical set-up was designed and computed using the finite element code ELEFANT (Thieulot, 2014; Lavecchia et al., 2017). Below, we review selected present-day subduction zones and their geometric characteristics as basis for our numerical model setting. Then, we summarize the rationale behind the hypothesis of van Hinsbergen et al. (2016) relating lateral variations in metamorphic grade recognized in the geology of western and central Turkey to oblique subduction. After that, we provide the results from a series of 3D numerical experiments and discuss the limitations of our simple experiments. We evaluate the implications of slab shape or trench geometry on the thermal regime of subduction zone and finally, compare the numerical results with geological examples Turkey as well as the Franciscan complex.

2 Oblique subduction: present and past examples

Many present-day subduction zones show an along-strike variability in the angle between the absolute motion direction of the downgoing plate and the trench. Fig. 1 shows that a majority of subduction zone have concave (e.g. Mariana; Sunda-Sumatra), or convex (central South America, Northeast Japan) shapes. The subduction rate along such curved subduction zones must

Solid Earth Discuss., https://doi.org/10.5194/se-2017-134
Manuscript under review for journal Solid Earth
Discussion started: 16 January 2018

change as a function of trench strike. This is best illustrated by the Aleutian trench (Fig. 1). In the eastern, NE-SW striking part of the trench, subduction is almost orthogonal, i.e. the plate motion of the downgoing Pacific plate is almost perpendicular to trench strike. In the western, NW-SE striking part of the Aleutian trench, there is almost no subduction and Pacific plate motion is almost parallel to the trench (e.g. Mccaffrey, 1992). This is also reflected in the westward decrease of the length of the Aleutian subducted slab (van der Meer et al., 2017). Consequently, the subduction rate along the Aleutian trench must gradually decrease from east to west upon increasing subduction obliquity.

If subduction rate is a primary control on the geotherm (e.g. van Keken et al., 2011), then along-strike variation in obliquity, should logically lead to along-strike changes in temperature at subduction interfaces. However, determining how strong these lateral variations may be is difficult to estimate from present-day subduction zones due to the lack of proxy to record it. Plank et al. (2009) provided a method to estimate temperature at the plate interface using melt-inclusions in arc volcanic rocks. Such data suggested along strike variations of temperature exist for example below Central America (Cooper et al., 2012). Better-constrained estimates for the temperature are available for paleo-subduction interfaces through studies of exhumed metamorphosed rocks in subduction-related orogens. These studies demonstrated that the thermal conditions in subduction zones varied through time (e.g. Agard et al., 2009; Plunder et al., 2015; Angiboust et al., 2016), but also along-strike. For instance, in the Franciscan complex of California (Wakabayashi and Dumitru, 2007), in the Sulawesi mélange in SE Asia (Parkinson, 1996), in the sub-ophiolitic melanges of Guatemala versus Cuba (Garcia-Casco et al., 2007), (garnet)-amphibolites are coeval with eclogite or blueschist along-strike in the same subduction complex. Taking the pressure (assumed to represent depth) of metamorphism into account, these may suggest along-strike temperature differences of *ca* 300°C. Less dramatic along strike temperature differences at similar depth of (*ca* 100°C) have also been recorded in Miocene subduction-related metamorphic rocks of Crete, Greece (Jolivet et al., 2010).

An extreme case of along-strike coeval metamorphic temperature variation was reconstructed from the geological record of Turkey. There, two belts of metamorphosed continental rock known as the Tavşanlı zone and the Kırşehir block experienced coeval metamorphism at strongly contrasting grades during their underthrusting/subduction below oceanic lithosphere that is preserved as ophiolites (e.g. Boztuğ et al., 2009; Plunder et al., 2013; van Hinsbergen et al., 2016). Part of these ophiolites are of supra-subduction zone type and formed ∼5-10 Myr before burial and metamorphism of the Kırşehir Block and Tavşanlı zone (van Hinsbergen et al., 2016, and references therein).

Both units were metamorphosed around 80-90 Ma (e.g. Whitney and Hamilton, 2004; Fornash et al., 2016; van Hinsbergen et al., 2016) within the same subduction system but under dramatically different metamorphic conditions. In the Tavşanlı zone peak metamorphic conditions were estimated to be around 24 ± 2 kbar and 500 ±50°C (Okay et al., 2002; Plunder et al., 2015), whereas peak metamorphism was estimated around 800 ± 100°C and 8 ± 1 kbar in the Kırşehir block (Whitney and Hamilton, 2004; Lefebvre et al., 2015). This would suggest that at similar depths, an along-strike temperature variation of more than 500°C existed (i.e. ∼200°C for the Tavşanlı zone at ∼25 km depths compared to 800°C for Kırşehir at the same depth).

The paleogeographic transition between the Tavşanlı and Kırşehir blocks has been deformed during later continent-continent collision processes, but appears to be abrupt, presently within tens of kilometres (Fig. 1b).

Paleogeographic and kinematic reconstructions of Central and Western Anatolia (Lefebvre et al., 2013; van Hinsbergen et al., 2016; Gürer et al., 2016), constrained based on structural geology and paleomagnetism, independent from interpretations of the causes of the contrast in metamorphism, suggest that the only major difference between the Tavşanlı and Kırşehir parts of the belt was the angle at which they were buried along the intra-oceanic trench below the oceanic lithosphere now found as ophiolites (Fig. 1b). Subduction of the belt was driven by ∼NNE-SSW convergence between Africa and Eurasia. The Tavşanlı zone was proposed to have been buried by near-orthogonal subduction along an ∼E-W trending trench segment, whereas the Kırşehir block would have been subducted highly obliquely (Fig. 1b) along a N-S striking trench segment, which was tentatively proposed to explain the stark metamorphic contrast (van Hinsbergen et al., 2016). Inspired by these geological examples and the hypothesis derived from those, we here aim to perform numerical experiments to test whether, and to what extent, the reconstructed thermal variations may be explained by along-strike variation in subduction geometry.

3 Model setting

3.1 Background

With increasing quality of geophysical measurement and network density, today's tomographic images allow to observe the geometry variation of slab geometry with depths (van der Meer et al., 2017). Such variations of slab shape are observed below the strait of Gibraltar (Bezada et al., 2013), below Turkey (Biryol et al., 2011), below Japan (Zhao et al., 2012; Liu and Zhao, 2016), below the eastern Caribbean plate (Van Benthem et al., 2013) and in many other subduction zones, and are summarized in the SLAB1.0 model (Hayes et al., 2012). These complicated pictures of slab geometry allow us to make simple tests to study the possible effects of geometry on the mantle flow and on temperature in subduction zones, and especially at the subduction interface.

Previous 3D thermo-kinematic numerical modeling studies have shown that variation of the geometry of the subduction zone may affect mantle flow patterns and may help to explain seismic anisotropy observed in subduction systems (e.g. Kneller and van Keken, 2007). Numerical models also suggested that the obliquity of subduction zones may have an effect on the temperature at the subduction interface (Bengtson and Van Keken, 2012; Morishige and van Keken, 2014; Ji and Yoshioka, 2015) but did not explore the relationship of such effects with the geological record. These studies have primarily shown that mantle flow may be related to the geometry of the slab edges that lead to the development of toroidal cells (i.e. with trench parallel material transport; Király et al., 2017; Schellart, 2017). Such trench-parallel, toroidal mantle flow has been proposed as a possible mechanism for differences in volcanic activity along subduction strike (Faccenna et al., 2010). Some mechanical studies have investigated the effect of trench geometry on the development of topography in the upper plate (e.g. Bonnardot et al., 2008). They also showed that plates bend in relation to the trench shape. Similar studies show that dynamic subduction systems develop 3D geometry with curvature as observed in nature, but in general such models are only mechanical and do not consider temperature (Pusok and Kaus, 2015; Király et al., 2017; Schellart, 2017), or the temperature pattern was not discussed

Solid Earth Discuss., https://doi.org/10.5194/se-2017-134
Manuscript under review for journal Solid Earth
Discussion started: 16 January 2018

in detail (Jadamec and Billen, 2010, 2012; Chertova et al., 2014). Hence, in our study, we aim to test to what extent trench geometry influences the geotherm of a subduction zone.

3.2 Numerical rationale and methods

The pioneering works of Batchelor (1967) and McKenzie (1969) allowed to investigate the thermal state of subduction zones by providing an analytical solution in 2D, whereby corner flow (i.e. poloidal flow) is dominant. Following these works, many studies were conducted on the behaviour of subduction zones using numerical approximations of corner flow, taking into account stress and temperature dependence of the material in the mantle wedge (e.g. van Keken et al., 2002, and ref therein). However no analytical solution exists in 3D for such problems. To investigate the effect of obliquity on mantle flow and on the temperature at the plate interface, we designed a simple numerical set-up using a reference model, and compute deviations from that reference for a set of models in which we vary trench shape. In addition, we briefly test the effect of subduction rate on the thermal state of the plate contact for the reference model. For geological cases where a plate subducts with an along strike varying obliquity it is then possible to add up the effects of trench geometry and subduction rate on mantle flow and therefore on the temperatures.

We used the finite element code ELEFANT (Thieulot, 2014; Lavecchia et al., 2017) to solve the mass, momentum and energy conservation equations in three-dimensions:

$$\boldsymbol{\nabla} \cdot \boldsymbol{v} = 0 \tag{1}$$

$$-\boldsymbol{\nabla} P + \boldsymbol{\nabla} \cdot (2\mu\dot{\varepsilon}) = 0 \tag{2}$$

$$\rho_0 C_p \left(\frac{\partial T}{\partial t} + \boldsymbol{v} \cdot \boldsymbol{\nabla} T \right) = \boldsymbol{\nabla} \cdot (k \boldsymbol{\nabla} T) \tag{3}$$

under the Boussinesq approximation with $\boldsymbol{v}$ the velocity, P the dynamic pressure, μ the effective viscosity, $\dot{\varepsilon}$ the strain-rate tensor, ρ the volumetric mass density, C_p the specific heat, T the absolute temperature, t the time and k the thermal conductivity. All values are given in table 1. The domain consists of a non-deforming upper plate, a slab with a kinematically prescribed velocity and an isoviscous dynamic mantle wedge. All coefficients were assumed to be constant both in time and space so that the temperature has no effect on the solution of Eqs. (1,2). As a consequence, once Eqs. (1,2) have been solved for a given set of boundary conditions and geometry, the same velocity field $\boldsymbol{v}$ is used to solve Eq. (3). This allows for a substantial reduction of the computational time since the discretisation of the Stokes equations yields a saddle point problem that is known to be much more computationally demanding than the energy system (Donea and Huerta, 2003).

Velocity boundary conditions were prescribed as shown in Fig. 2 and are summarized as follows: (i) a subduction rate of 4 cm.yr^{-1} was imposed with a dip angle of $45°$ for the slab (Fig. 2), a combination that is reasonable considering present-day subduction zones (Syracuse et al., 2010) and that is similar to reconstructed Africa-Europe convergence rates around 90-80 Ma

Solid Earth Discuss., https://doi.org/10.5194/se-2017-134
Manuscript under review for journal Solid Earth
Discussion started: 16 January 2018

(Seton et al., 2012), and thus applicable to the case study of Anatolia. (ii) the top 32 km of the mantle wedge was assumed to be rigid to mimic the mechanical behaviour and the thickness of a 5 million year old crust and shallow lithosphere, similar to the Anatolian case study; (iii) no in- or out-flow was allowed in the direction parallel to the trench ($v_y = 0$); (iv) no vertical movement was allowed in the rear of the modeling space.

The temperature at the surface was set to 0°C. At the front and the rear of the domain, the temperature was computed using a half space cooling model that is in good agreement with various geophysical observations for oceanic lithosphere younger that 60 My (Turcotte (1987) and references therein). The age was set to 25 My for the subducting plate and as a 5 My old lithosphere for the upper plate. In the rear of the modeling space, the thermal state is prescribed until reaching the in/out flow transition at 100 km depth (Fig. 1).

The computational domain is discretized on a grid counting $65 \times 85 \times 65 = 359,125$ elements. In all calculations we used linear Q_1Q_1 elements for velocity, pressure and temperature. Since equal-order-interpolation for the velocity-pressure pair is known to yield an unstable mixed finite element formulation. We used the stabilization method of Dohrmann and Bochev (2004) that was previously successfully implemented in other geodynamic models (Stadler et al., 2010; Burstedde et al., 2013). We also user a preconditioned Conjugate Gradient method to solve the Schur complement of the Stokes system (inner solves are carried out with the direct solver MUMPS () while we used a GMRES solver for the energy equation finite element matrix. Calculations were run on a Desktop machine on a single processor and each model took about one hour to compute.

3.3 Geometry of the models

At the beginning of each simulation the grid was built as a Cartesian box and then deformed to conform to the required curved geometry and boundary conditions imposed. The position x_t of the trench as a function of the y coordinate is prescribed by means of a sine or an arctangent function:

$$x_t(y) = x + A\left[1 - \left(\sin\frac{y - \frac{Ly}{2}}{L_y}\pi\right)^{2\beta}\right] \tag{4}$$

$$x_t(y) = x + A\left[\arctan\left(\gamma\left(\frac{y}{L_y} - \frac{1}{2}\right)\right)\right] \tag{5}$$

where A is the amplitude of the curvature and β and γ are parameters controlling its shape. The angle between the trench and the direction of convergence, parallel to x, is called θ and varies with y (Fig. 2).

4 Results

The models are named after the parameters controlling the shape of their trench (A, β or γ; see Eqs. 4 or 5; e.g. SINA_β). Model SIN20_1 will be described in detail and serves as a reference against which other runs are compared. This model has a sinusoidal shape with an amplitude of 20 km and a β value of 1. For all the convex models, the maximum obliquity (θ_{max}) is reported in Table 2. For all the experiments the value of θ_{max} is indicated on the figure describing the experiment. We provide movies of all models in supplementary materials.

4.1 Boundary conditions in the rear of the model

Two different types of boundary conditions were investigated for the rear of the box: (i) the in/out flow is allowed only in the x direction (with $v_y = 0, v_z = 0$) (ii) the in/out flow allowed in the x and y direction (with only $v_z = 0$). At 60 kilometres depth the difference in the mantle wedge flow is minimal when the subducting slab is far from the rear of the box. There, the maximum v_y value is 1.41 mm/yr and 1.54 mm/yr with the (i) and (ii) boundary condition respectively, i.e. a $\sim 8\%$ difference. At depths of 75 and 90 kilometres and closer to the rear of the modeling space this difference increases to 13% and 26%, respectively. We chose de second approach to be more realistic in what floows.

4.2 Description of the reference experiment: SIN20_1

4.2.1 Mantle wedge flow

The 3D velocity pattern of the mantle wedge is shown using streamlines coloured with trench-parallel velocity v_y (Fig. 3) and cross sections at different depth intervals (60, 75 and 90 km). In our computation we observe that the shape of the box influences the mantle wedge flow (i.e. the geometry of the trench and slab). Some inflow of mantle comes from the backarc region and is dragged at depth due to the viscous coupling with the subducting slab. This is especially true in the middle and edges of the box where the obliquity angle is null. This is shown on the top and rear view of the model (Fig. 3a,b) where the mantle flow on both sides and in the middle does not depict a trench parallel component. In the inflow area the trench-parallel component of the velocity is close to zero (0.05 mm/yr). The material is drawn in in the arc region and transported linearly towards the subduction area. In the narrower part of the wedge, the trench-parallel component of the velocity increases up to 2.9 mm/yr reaching there a maximum when the obliquity angle is maximum (at 64 km from the edge on the reference model SIN20_1; Fig. 3a, cross section). It almost corresponds to the location where the flow reverses and where the velocity is of ∼5 mm/yr. Along the subducting plate, the mantle flow follows the interface. The streamlines are affected by some trench-parallel flow around the maximum curvature region (y = 64 km and y = 128 km; Fig. 3a,b). There, the y component of the velocity is to maximum 2.54 mm/yr being almost negligible compared to a magnitude velocity up to 30.0 mm/yr (v_y = ∼2.9% of $\boldsymbol{v}$). In the outflow area the average magnitude velocity is 12.6 mm/yr. It is mostly composed of the x component ($\overline{v}_x$ = 12.5 mm/yr) and the y component corresponds to ∼12% on average the total velocity ($\overline{v}_y$ = 1.20 mm/yr). In the wedge, the y component of the velocity is maximum at a position equivalent to 1/4 of the box size (i.e. where $\theta \rightarrow \theta_{max}$; Fig. 3a,b). Its value is 1.54 mm/yr at 60 km depth, 1.42 mm/yr at 75 km and 0.94 mm/yr at 90 km depth. This corresponds to ∼12%, ∼16% and ∼17% of the magnitude velocity $v_{mag} = |\boldsymbol{v}|$ at the same location respectively (Fig. 3d,e,f and Table 2).

In summary, a trench parallel flow develops in the mantle wedge in relation with the shape of the trench. The trench parallel component of the flow cancels at the centre of the model and adds up to the along plate interface flow to transport more material at depth.

4.2.2 The thermal structure

The thermal structure is presented in a 3D view and as map views across the mantle wedge at different depths (Fig. 3c,g,h,i). In addition, depth-temperature paths measured along the plate interface are provided but only shown for one half of the model because they are symmetric. As discussed before, the velocity field converges towards the centre of the modeling space (Fig. 4). Due to advection it appears logical that the 450°C isotherm is deflected downward in the centre of the modeling space (i.e. where the trench parallel velocity become zero; Fig. 3c). As a consequence the thermal regime of the subduction zone is different along strike and is cooler in the middle of the domain.

This is also well illustrated with the depth-temperature path along the interface (Fig. 4). Fig. 4 illustrates that the path in the centre of the model is the coldest and that paths at the edges are the warmest. For this reference model the along-strike variation of temperature at the subduction interface is 50°C at a depth of 75 km (See inset on Fig. 4). This variation becomes smaller at shallower depth when the subduction interface gets closer to the fixed overriding plate. This region namely the cold nose is even sometimes considered as fixed (e.g. van Keken et al., 2002).

4.2.3 The effect of velocity on the thermal structure

A set of additional experiments with varying subduction rates was also calculated with velocity of 2 and 7 cm/yr for the reference concave model. With 2 cm/yr, the geotherm of the subduction zone gets about 50°C warmer. With 7 cm/yr the global geotherm gets 50°C colder. In both cases a difference of ∼50°C is observed between the centre and the edges of the model at 75 km depths (Fig. 4).

4.3 Summary of the other experiments

4.3.1 Convex and concave models

Convex models: The maximum value of θ is measured either at ~ 42 or 64 km (according to the value at which the second derivative of eq. 4 equals zero). As in the reference experiment, the mantle wedge flow shows a trench parallel velocity with a increasing value in the region where the obliquity is the highest. The maximum trench parallel velocity is reported in table 2 for all convex experiments. It accounts for up to 50% of the magnitude velocity in the model with the biggest amplitude ($A = 60$km) and $\beta = 1$. When $\beta = 2$ and with the maximum amplitude, the trench parallel velocity may even account for 95% of the total velocity field (Fig. 5; Table 2). This trench parallel component of the velocity field is sufficient to allow transportation of heat and creates a symmetric pattern in the temperature field with a colder slab in the middle of the experiment. Our calculations show a difference of temperature of up to 110°C for the most extreme configuration tested (i.e. $\theta = 36°$; Fig. 5a,c).

Variation of the curvature: When varying the wavelength of the curvature of the experiments (e.g. set of experiments SIN40_2, SIN60_2, -SIN40_2, -SIN60_2) the mantle flow pattern and thermal structure also show trench parallel variations. As in the reference model SIN20_1, the mantle flow is affected by the shape of the slab and shows some maximum trench

Solid Earth Discuss., https://doi.org/10.5194/se-2017-134
Manuscript under review for journal Solid Earth
Discussion started: 16 January 2018

velocity perturbation where the obliquity is maximum (e.g. 30°). This leads (1) to a difference in the velocity field, with v_y representing up to 50% of the total velocity at 75 km depth and (2) to a variation of the plate interface temperature of more than 100°C (Fig. 5c). This difference of temperature is observed in a distance of less that a hundred kilometres and is due to the strong trench parallel component of the mantle flow. Interestingly the coldest thermal regime in the convex models does not correspond to the edge of the modeling space where no trench parallel flow is allowed (see boundary condition on Fig. 2) but rather to the centre. This is due to massive transport of mantle material towards the centre of the convex slab.

Concave models: In the concave models, the mantle flow is directed towards the edges of the modeling space with a non-negligible trench parallel velocity. As a consequence, the coldest part of the model is located at the borders of the modeling space because mantle material is transported towards the model edges (Fig. 5b). The geometry of the modeling space is symmetric, similar to the reference model. It implies that the velocity field is also a symmetric expression of the one observed in the reference model (See Fig. 5b).

4.3.2 S-shaped models

The models described hereafter are named ATANA_ γ with reference to the parameters of Eq. 5. The maximum obliquity angle (see Eq. 5) is by definition located in the center of the model space. Its value evolves from 21° to 38° in our experiments. As seen in the previous section the shape of the box influences the pattern of the mantle corner flow. For all presented boxes, the mantle flow shows some deviation towards the right as depicted by the white arrows on the 3D view (Fig. 6: 3D views and v_y maps) with a maximum trench parallel flow where the curvature is the most important. The trench-parallel velocity goes up to 8.0 mm/yr in model ATAN40_05, up to 1.8 mm/yr in model ATAN05_20 and up to 3.5 mm/yr in model ATAN10_20. It corresponds respectively to ~83%, ~35% and ~17% of the magnitude velocity at the same location. This differences in the velocity field lead to differences in the temperature field represented on slices at 75 km depth and as depth-temperature path. Contrary to the convex and concave models, the temperature solution presented here is asymmetric as seen on the isotherm plotted on the slices at 75 kilometres depth and on the depth–temperature paths. It shows some important variation of the temperature along strike of the subduction zone too and this behaviour is in agreement with the asymmetric mantle flow.

We computed the maximum temperature difference between the centre and side of the model to be of 200°C for models ATAN40_05 and ATAN05_20. In model ATAN40_05 the shape of the 450°C isotherm is relatively smooth whereas in model ATAN05_20 it is sharper in direct relation with the shape of the trench. It shows that similar differences of temperature along strike can be obtained with different geometries. The model ATAN05_20 only has a difference of 75°C between the middle and the coldest edge and the step of the 450°C isotherm is minimal, illustrating that increasing obliquity leads to increasing temperature variations.

Solid Earth Discuss., https://doi.org/10.5194/se-2017-134
Manuscript under review for journal Solid Earth
Discussion started: 16 January 2018

5 Discussion

5.1 Implications of obliquity in subduction systems

We now evaluate the implications of our results for along-strike temperature variations in subduction zones with obliquity variations that consume a single plate. Our numerical experiments show a straightforward link between mantle wedge flow, the temperature at the plate interface, and the geometry of the subducting slab due to trench shape. This is observed for all type of geometries that we explored (convex, concave, S-shaped). The geometry affects the mantle wedge flow and adds a toroidal flow component to the dominant poloidal flow. This toroidal flow affects the temperature pattern at the plate interface. The temperature difference may become as much as ~200°C in models with an obliquity of ~40° (model ATAN40_05 or ATAN10_20; Fig. 6). These results agree well with previous numerical modeling work (Bengtson and Van Keken, 2012; Morishige and van Keken, 2014; Ji and Yoshioka, 2015; Wada et al., 2015). Our systematic study of the influence of the shape of the trench on the geotherm shows that a larger amplitude in the model (convex of concave) leads to a larger trench parallel flow and consequently a larger difference in the temperature at the plate interface. The S-shaped model is particularly interesting as it shows that even a small difference in geometry will be expressed as a trench parallel flow and a change of the temperature. The thermal regime is thought to be controlled by the angle of the subduction and the velocity and age of the downgoing plate, known as the Φ parameter ($\Phi = AV_n sin(\delta)$; with A the age of the incoming lithosphere, V_n the normal velocity of the incoming plate and δ the subduction angle; Kirby et al., 1991). Following our experiments, Φ remains certainly the first order parameter but we demonstrate that the trench parallel mantle flow influences on the temperature at the plate interface and may thus explain along-strike temperature differences in subduction zones. A 2D approach remains viable in systems with small obliquity, as stated in Bengtson and Van Keken (2012), but important variations of geometry should be considered in further studies to reliably represent subduction zone dynamics both for present-day and past systems.

5.2 Limitations

The experiments with an amplitude variation of 20, 40 or 60 km over 250 km display a substantial effect on the mantle wedge flow and temperature pattern at the plate interface. Such geometrical variations are observed on Earth (e.g. in the Andean subduction around the border between Chile and Peru, or below Japan (Fig. 1)). However, our modelling apporach is not without limitations: first, our modell setting is a highly simplified geometry of a subduction zone; second, in our kinematic approach the deformation (especially at the interface) is not taken in account; third, the isoviscous rheology we use is known to underestimates the temperature predicted in the mantle wedge (van Keken et al., 2002). In addition no feedback mechanisms induced by effects of temperature change along the plate interface, such as water transport or melting processes that may influence the mechanical behaviour, were taken in account. We made these simplifications because it allows for a dramatically lower computation time and was useful to evaluate the qualitative effect of the geometry on the thermal regime. We primarily aimed to test whether the major contemporaneous along-strike changes in temperature in geological records of subduction zones may be to first order explained by subduction obliquity changes, and our results suggest that they may indeed. Our study may thus form the basis for more detailed studies on the effect of obliquity on e.g. dehydration reaction and seismicity in subduction zones as function of obliquity, taking the effects of above limitations into account.

5.3 Comparison with the geological record

We now compare our models to the geologically constrained temperature variations in paleo-subduction zones. Our study was largely motivated by the geological record from Western and Central Turkey, but as mentioned, similar along-strike temperature variations have been recovered from other geological settings such as the Fanciscan complex (see review by Wakabayashi, 2015, 2017), the Sulawesi mélange (Parkinson, 1996), or the peri-Caribbean mélanges (Garcia-Casco et al., 2007). In all settings along-strike metamorphic grade variation were recorded at similar times within the same subduction system. Our model results suggest that variations in subduction obliquity, may tip a subduction interface from a (cold) gradient through the lawsoinite blueschist facies to a (warm) gradient through the amphibole eclogite facies as calculated by Hacker et al. (2003a). Our models do not reproduce the extreme case of Anatolia, where the along-strike temperature variation at 30 km depth may have been as high as 500°C. However the reconstructed angle between the western and central Anatolian subduction segments may have been as much as 90°(Lefebvre et al., 2013; van Hinsbergen et al., 2016), and perhaps that extreme angle may explain the very high temperature gradient, although other factors, e.g. related to the continental nature of the downgoing plate, may have played a role.

The influence of the mantle wedge convection pattern is interesting in terms of general understanding of subduction mechanism, their geochemical or geophysical structures and possibly their evolution. From a geological perspective it is interesting to reconcile field observation with models. Penniston-Dorland et al. (2015) argued that "rocks are hotter than models" but since the shape of the subduction zone has an effect on the temperature at the plate interface (e.g Bengtson and Van Keken, 2012; Morishige and van Keken, 2014, this study) such differences may only be an artefact of the 2D geometry used in their study. Some models have shown that there is a strong competition between toroidal and poloidal flow around slab edges and that the velocity of the flow can be relatively large (Jadamec and Billen, 2010; Király et al., 2017). Jadamec and Billen (2012) even showed that the difference between the horizontal velocity field using linear, composite and non-linear rheologies may be an order of magnitude. Such changes in the velocity field would probably lead to differences in the temperature field itself and definitely increase the plate interface temperature. Modeling mantle flow accounting for differences in temperature is also of interest in the light of the *in-situ* record of temperature of the slab from melt-inclusion in arc eruptive volcanic rocks using geochemistry (Plank et al., 2009; Cooper et al., 2012). Such data suggest along strike-temperature variations may exist below Central America, Cascadia or the Mariannas. Finally, the obliquity effect is worth taking into account when assessing e.g. megathrust seismic hazards in link with dehydration reaction and events such as the episodic tremor and slip thought to represent fluid pulses along the interface in response to dehydration events (Rogers and Dragert, 2003; Audet and Kim, 2016).

In any case, the simple numerical modeling performed in this contribution positively tests our hypothesis that along-strike variation in subduction obliquity may have a first-order control on the temperature at the subduction interface, and may help

Solid Earth Discuss., https://doi.org/10.5194/se-2017-134
Manuscript under review for journal Solid Earth
Discussion started: 16 January 2018

us to understand the variation of geothermal gradient along strike of subduction zones, such as predicted by surface heat flow, for example below Japan (Tanaka, 2004). In light of the presented numerical models we argue that the plate boundary configuration may play a prime role in inducing strong lateral variations in geotherm within subduction systems, e.g. along the Aleutian trench, at kinks such as in Alaska or Kamchatka, and along the southern Marianas or northern Caribbean trenches.

6 Conclusions

Today's configuration of subduction zones, as well as plate tectonic reconstructions, show major along-strike variations in subduction obliquity along trenches. Here, we study the effect of trench geometry on temperatures at the subduction interface. To this end, we performed a series of simple numerical experiments with concave, convex and S-shaped subduction zones. Our results show that along-strike obliquity affects the geotherm of the subduction zone in two ways: by inducing a component of toroidal flow, and by changing the rate of subduction, both increasing temperatures at subduction zones with increasing obliquity. We compute along-strike temperature differences at 30-90 km depth that may be 200°C or more, depending on the geometry. This may be added to the well-known effects of subducting plate age to account for even larger temperature variations. On the other hand, our study did not take into account any feedback mechanisms induced by e.g. fluid flow or deformation, which may modify our estimates. In any case, we demonstrate that oblique trenches have the propensity to higher geotherms. Our results may provide a basis to explain geological record of coeval metamorphic rocks that formed at the same subduction interface, but under very different pressure-temperature conditions (e.g. in Turkey, SE Asia, California). In addition, our study may be of importance for assessing the thermal regime of present-day subduction zones linked to melting processes and seismic hazards.

Author contributions. AP and CT designed the experiments and AP carried them out. CT developed the finite element code ELEFANT. AP prepared the manuscript with contributions from all co-authors.

Acknowledgements. We thank Luuk Schuurmans for investigating a few aspect of the presented research. Prof. Riad Hassani is warmly thanked for his help with the implementation of the stabilised Q_1Q_1 finite element formulation in ELEFANT. AP and DJJvH were funded through ERC starting grant SINK (306810). DJJvH acknowledges NWO Vidi grant 864.11.004. The perceptually-uniform colour maps davos and vik were used in this study to prevent visual distortion of the data http://www.fabiocrameri.ch/visualisation.php.

References

Agard, P., Yamato, P., Jolivet, L., and Burov, E. (2009). Exhumation of oceanic blueschists and eclogites in subduction zones: Timing and mechanisms. *Earth-Science Reviews*, 92(1-2):53–79.

Amestoy, P., Guermouche, A., L'Excellent J.-Y., and Pralet S. (2006) A Fully Asynchronous Multifrontal Solver Using Distributed Dynamic Scheduling *SIAM Journal on Matrix Analysis and Applications, 23:15–41.*

Amestoy, P., Guermouche, A., L'Excellent J.-Y., and Pralet S. (2006) Hybrid scheduling for the parallel solution of linear systems *Parallel Computing, 2:136–156.*

Angiboust, S., Agard, P., Glodny, J., Omrani, J., and Oncken, O. (2016). Zagros blueschists: Episodic underplating and long-lived cooling of a subduction zone. *Earth and Planetary Science Letters*, 443:48–58.

Argus, D. F., Gordon, R. G., and Demets, C. (2011). Geologically current motion of 56 plates relative to the no-net-rotation reference frame. *Geochemistry, Geophysics, Geosystems*, 12(11):1–13.

Audet, P. and Kim, Y. (2016). Teleseismic constraints on the geological environment of deep episodic slow earthquakes in subduction zone forearcs: A review. *Tectonophysics*, 670:1–15.

Batchelor, G. K. (1967). An Introduction to Fluid Dynamics. *Cambridge Univ. Press, New York*, page 615.

Bengtson, A. K. and Van Keken, P. E. (2012). Three-dimensional thermal structure of subduction zones: Effects of obliquity and curvature. *Solid Earth*, 3(2):365–373.

Bezada, M. J., Humphreys, E. D., Toomey, D. R., Harna, M., Dávila, J. M., and Gallart, J. (2013). Evidence for slab rollback in westernmost Mediterranean from improved upper mantle imaging. *Earth and Planetary Science Letters*, 368:51–60.

Bird, P. (2003). An updated digital model of plate boundaries. *Geochemistry, Geophysics, Geosystems*, 4(3).

Biryol, B., Beck, S. L., Zandt, G., and Özacar, A. A. (2011). Segmented African lithosphere beneath the Anatolian region inferred from teleseismic P-wave tomography. *Geophysical Journal International*, 184(3):1037–1057.

Bonnardot, M. A., Hassani, R., Tric, E., Ruellan, E., and R??gnier, M. (2008). Effect of margin curvature on plate deformation in a 3-D numerical model of subduction zones. *Geophysical Journal International*, 173(3):1084–1094.

Bouilhol, P., Magni, V., van Hunen, J., and Kaislaniemi, L. (2015). A numerical approach to melting in warm subduction zones. *Earth and Planetary Science Letters*, 411:37–44.

Boztuğ, D., Jonckheere, R., Heizler, M., Ratschbacher, L., Harlavan, Y., and Tichomirova, M. (2009). Timing of post-obduction granitoids from intrusion through cooling to exhumation in central Anatolia, Turkey. *Tectonophysics*, 473(1-2):223–233.

Burstedde, C., Stadler, G., Alisic, L., Wilcox, L., Tan, E., Gurnis, M., and Ghattas, O. (2013). Large-scale adaptive mantle convection simulation. *GJI*, 192:889–906.

Chertova, M. V., Spakman, W., Geenen, T., Van Den Berg, A. P., and Van Hinsbergen, D. J. J. (2014). Underpinning tectonic reconstructions of the western Mediterranean region with dynamic slab evolution from 3-D numerical modeling. *Journal of Geophysical Research: Solid Earth*, 119(7):5876–5902.

Cooper, L. B., Ruscitto, D. M., Plank, T., Wallace, P. J., Syracuse, E. M., and Manning, C. E. (2012). Global variations in H2O/Ce: 1. Slab surface temperatures beneath volcanic arcs. *Geochemistry, Geophysics, Geosystems*, 13(3).

Dohrmann, C. and Bochev, P. (2004). A stabilized finite element method for the Stokes problem based on polynomial pressure projections. *Int. J. Num. Meth. Fluids*, 46:183–201.

Donea, J. and Huerta, A. (2003). *Finite Element Methods for Flow Problems*. John Wiley & Sons.

Faccenna, C., Becker, T. W., Lallemand, S., Lagabrielle, Y., Funiciello, F., and Piromallo, C. (2010). Subduction-triggered magmatic pulses: A new class of plumes? *Earth and Planetary Science Letters*, 299(1-2):54–68.

Fornash, K. F., Cosca, M. A., and Whitney, D. L. (2016). Tracking the timing of subduction and exhumation using 40Ar/39Ar phengite ages in blueschist- and eclogite-facies rocks (Sivrihisar, Turkey). *Contributions to Mineralogy and Petrology*, 171(7):67.

Garcia-Casco, A., Lazaro, C., Rojas-Agramonte, Y., Kroner, A., Torres-Roldan, R. L., Nunez, K., Neubauer, F., Millan, G., and Blanco-Quintero, I. (2007). Partial Melting and Counterclockwise P T Path of Subducted Oceanic Crust (Sierra del Convento Melange, Cuba). *Journal of Petrology*, 49(1):129–161.

Gorczyk, W., Gerya, T. V., Connolly, J. A. D., and Yuen, D. A. (2007). Growth and mixing dynamics of mantle wedge plumes. *Geology*, 35(7):587–590.

Gürer, D., Hinsbergen, D. J. J., Matenco, L., Corfu, F., and Cascella, A. (2016). Kinematics of a former oceanic plate of the Neotethys revealed by deformation in the Ulukışla basin (Turkey). *Tectonics*, pages 1–32.

Hacker, B. R., Abers, G. A., and Peacock, S. M. (2003a). Subduction factory 1. Theoretical mineralogy, densities, seismic wave speeds, and H2O contents. *Journal of Geophysical Research*, 108(B1):2029.

Hacker, B. R., Peacock, S. M., Abers, G. A., and Holloway, S. D. (2003b). Subduction factory 2. Are intermediate-depth earthquakes in subducting slabs linked to metamorphic dehydration reactions? *Journal of Geophysical Research*, 108(B1):2030.

Hayes, G. P., Wald, D. J., and Johnson, R. L. (2012). Slab1.0: A three-dimensional model of global subduction zone geometries. *Journal of geophysical research*, 117:1–15.

Honda, S. and Yoshida, T. (2005). Effects of oblique subduction on the 3-D pattern of small-scale convection within the mantle wedge. *Geophysical Research Letters*, 32(13):1–4.

Jadamec, M. A. and Billen, M. I. (2010). Reconciling surface plate motions with rapid three-dimensional mantle flow around a slab edge. *Nature*, 465(7296):338–341.

Jadamec, M. A. and Billen, M. I. (2012). The role of rheology and slab shape on rapid mantle flow : Three-dimensional numerical models of the Alaska slab edge. *Journal of Geophysical Research*, 117(February):1–20.

Ji, Y. and Yoshioka, S. (2015). Effects of slab geometry and obliquity on the interplate thermal regime associated with the subduction of three-dimensionally curved oceanic plates. *Geoscience Frontiers*, 6(1):61–78.

Johnston, S. T. (2001). The Great Alaskan Terrane Wreck: Reconciliation of paleomagnetic and geological data in the Northern Cordillera. *Earth and Planetary Science Letters*, 193(3-4):259–272.

Jolivet, L., Trotet, F., Monié, P., Vidal, O., Goffé, B., Labrousse, L., and Agard, P. Along-strike variations of P–T conditions in accretionary wedges and syn-orogenic extension , the HP–LT Phyllite–Quartzite Nappe in Crete and the Peloponnese *Tectonophysics, 480:133–148*

Király, Á., Capitanio, F. A., Funiciello, F., and Faccenna, C. (2017). Subduction induced mantle flow: Length-scales and orientation of the toroidal cell. *Earth and Planetary Science Letters*, 479:284–297.

Kirby, S., Engdahl, R. E., and Denlinger, R. (1996). *Intermediate-depth intraslab earthquakes and arc volcanism as physical expressions of crustal and uppermost mantle metamorphism in subducting slabs*, volume 96 of *Geophysical Monograph Series*. American Geophysical Union, Washington, D. C.

Kirby, S. H., Durham, W. B., and Stern, L. A. (1991). Mantle Phase Changes and Deep-Earthquake faulting in subducting lithosphere. *Science*, 252:216–225.

Kneller, E. a. and van Keken, P. E. (2007). Trench-parallel flow and seismic anisotropy in the Mariana and Andean subduction systems. *Nature*, 450(7173):1222–1225.

Kneller, E. A. and van Keken, P. E. (2008). Effect of three-dimensional slab geometry on deformation in the mantle wedge: Implications for shear wave anisotropy. *Geochemistry, Geophysics, Geosystems*, 9(1):n/a–n/a.

Lavecchia, A., Thieulot, C., Beekman, F., Cloetingh, S., and Clark, S. (2017). Lithosphere erosion and continental breakup : Interaction of extension , plume upwelling and melting. *Earth and Planetary Science Letters*, 467:89–98.

Lefebvre, C., Meijers, M. J., Kaymakci, N., Peynircioğlu, A., Langereis, C. G., and van Hinsbergen, D. J. (2013). Reconstructing the geometry of central Anatolia during the late Cretaceous: Large-scale Cenozoic rotations and deformation between the Pontides and Taurides. *Earth and Planetary Science Letters*, 366:83–98.

Lefebvre, C., Peters, K., Wehrens, P. C., Brouwer, F. M., and van Roermund, H. L. (2015). Thermal history and extensional exhumation of a high-temperature crystalline complex (Hırkadağ Massif, Central Anatolia). *Lithos*, 238:156–173.

Liu, L., Spasojevic, S., and Gurnis, M. (2008). Reconstructing Farallon Plate Subduction Beneath North America Back to the Late Cretaceous. *Science*, 328(March):1907–1912.

Liu, X. and Zhao, D. (2016). P and S wave tomography of Japan subduction zone from joint inversions of local and teleseismic travel times and surface-wave data. *Physics of the Earth and Planetary Interiors*, 252:1–22.

Mccaffrey, R. (1992). Oblique plate convergence, slip vectors, and forearc deformation. *Journal of Geophysical Research*, 97(92):8905–8915.

McKenzie, D. P. (1969). Speculations on the consequences and causes of plate motions. *Geophys. J. Roy. Astron. Soc.*, 18(1608):1–32.

Menant, A., Sternai, P., Jolivet, L., Guillou-Frottier, L., and Gerya, T. (2016). 3D numerical modeling of mantle flow, crustal dynamics and magma genesis associated with slab roll-back and tearing: The eastern Mediterranean case. *Earth and Planetary Science Letters*, 442:93–107.

Morishige, M. and van Keken, P. (2014). Along-arc variation in the 3-D thermal structure around the junction between the Japan and Kurile arcs. *Geochemistry Geophysics Geosystems*, 18:1–16.

Okay, A. I., Monod, O., and Monie, P. (2002). Triassic blueschists and eclogites from northwest Turkey : vestiges of the Paleo-Tethyan subduction. *Lithos*, 64:155–178.

Parkinson, C. D. (1996). The origin and significance of metamorphosed tectonic blocks in mélanges: Evidence from Sulawesi, Indonesia. *Terra Nova*, 8(4):312–323.

Peacock, S. M. and Wang, K. (1999). Seismic Consequences of Warm Versus Cool Subduction Metamorphism: Examples from Southwest and Northeast Japan. *Science*, 286:937–939.

Penniston-Dorland, S. C., Kohn, M. J., and Manning, C. E. (2015). The global range of subduction zone thermal structures from exhumed blueschists and eclogites: Rocks are hotter than models. *Earth and Planetary Science Letters*, 428:243–254.

Plank, T., Cooper, L. B., and Manning, C. E. (2009). Emerging geothermometers for estimating slab surface temperatures. *Nature Geoscience*, 2(9):611–615.

Plunder, A., Agard, P., Chopin, C., and Okay, A. (2013). Geodynamics of the Tavşanlı zone , western Turkey: Insights into subduction / obduction processes. *Tectonophysics*, 608:884–903.

Plunder, A., Agard, P., Chopin, C., Pourteau, A., and Okay, A. I. (2015). Accretion, underplating and exhumation along a subduction interface: From subduction initiation to continental subduction (Tavşanlı zone, W. Turkey). *Lithos*, 226:233–254.

Pusok, A. E. and Kaus, B. J. P. (2015). Development of topography in 3-D continental-collision models. *Geochemistry, Geophysics, Geosystems*, pages 1378–1400.

Rogers, G. and Dragert, H. (2003). Episodic tremor and slip on the Cascadia subduction zone: the chatter of silent slip. *Science*, 300:1942–1943.

Ryan, W. B., Carbotte, S. M., Coplan, J. O., O'Hara, S., Melkonian, A., Arko, R., Weissel, R. A., Ferrini, V., Goodwillie, A., Nitsche, F., Bonczkowski, J., and Zemsky, R. (2009). Global multi-resolution topography synthesis. *Geochemistry, Geophysics, Geosystems*, 10(3).

Schellart, W. P. (2017). Andean mountain building and magmatic arc migration driven by subduction-induced whole mantle flow. *Nature Communications*, 8(1):2010.

Schepers, G., Van Hinsbergen, D. J., Spakman, W., Kosters, M. E., Boschman, L. M., and McQuarrie, N. (2017). South-American plate advance and forced Andean trench retreat as drivers for transient flat subduction episodes. *Nature Communications*, 8(0316):1–9.

Seton, M., Müller, R., Zahirovic, S., Gaina, C., Torsvik, T., Shephard, G., Talsma, a., Gurnis, M., Turner, M., Maus, S., and Chandler, M. (2012). Global continental and ocean basin reconstructions since 200Ma. *Earth-Science Reviews*, 113(3-4):212–270.

Stadler, G., Gurnis, M., Burstedde, C., Wilcox, L., Alisic, L., and Ghattas, O. (2010). The dynamics of plate tectonics and mantle flow: from local to global scales. *Science*, 329:1033–1038.

Stampfli, G. M. and Borel, G. D. (2002). A plate tectonic model for the Paleozoic and Mesozoic constrained by dynamic plate boundaries and restored synthetic oceanic isochrons. *Earth and Planetary Science Letters*, 196(1-2):17–33.

Syracuse, E. M., van Keken, P. E., and Abers, G. A. (2010). The global range of subduction zone thermal models. *Physics of the Earth and Planetary Interiors*, 183(1-2):73–90.

Tanaka, A. (2004). Geothermal gradient and heat flow data in and around Japan (II): Crustal thermal structure and its relationship to seismogenic layer. *Earth, Planets and Space*, 56(12):1195–1199.

Thieulot, C. (2014). ELEFANT: a user-friendly multipurpose geodynamics code. *Solid Earth*, 6:1949–2096.

Turcotte, D. L. (1987). Rheology of the oceanic and continental lithosphere. In *Composition, Structure and Dynamics of the Lithosphere-Asthenosphere System*, volume 16, pages 61–67. American Geophysical Union.

Turcotte, D. L. and Schubert, G. (2014). Geodynamics, third edition.

Van Benthem, S., Govers, R., Spakman, W., and Wortel, R. (2013). Tectonic evolution and mantle structure of the Caribbean. *Journal of Geophysical Research: Solid Earth*, 118(6):3019–3036.

van der Meer, D. G., van Hinsbergen, D. J. J., and Spakman, W. (2017). Atlas of the underworld: Slab remnants in the mantle, their sinking history, and a new outlook on lower mantle viscosity. *Tectonophysics*.

van Hinsbergen, D. J. J., Maffione, M., Plunder, A., Kaymakcı, N., Ganerød, M., Hendriks, B. W. H., Corfu, F., Gürer, D., de Gelder, G., Peters, K., McPhee, P., Brouwer, F. M., Advokaat, E. L., and Vissers, R. L. (2016). Tectonic evolution and paleogeography of the Kırşehir Block and the Central Anatolian Ophiolites, Turkey. *Tectonics*, 35:983–1014.

van Keken, P. E., Hacker, B. R., Syracuse, E. M., and Abers, G. A. (2011). Subduction factory: 4. Depth-dependent flux of H2O from subducting slabs worldwide. *Journal of Geophysical Research*, 116(B1):B01401, doi:10.1029/2010JB007922.

van Keken, P. E., Kiefer, B., and Peacock, S. M. (2002). High-resolution models of subduction zones: Implications for mineral dehydration reactions and the transport of water into the deep mantle. *Geochemistry Geophysics Geosystems*, 3(10):1056.

Vérard, C., Flores, K., and Stampfli, G. (2012). Geodynamic reconstructions of the South America-Antarctica plate system. *Journal of Geodynamics*, 53(1):43–60.

Wada, I., Behn, M. D., and Shaw, A. M. (2012). Effects of heterogeneous hydration in the incoming plate, slab rehydration, and mantle wedge hydration on slab-derived H 2O flux in subduction zones. *Earth and Planetary Science Letters*, 353-354:60–71.

Wada, I., He, J., Hasegawa, A., and Nakajima, J. (2015). Mantle wedge flow pattern and thermal structure in Northeast Japan: Effects of oblique subduction and 3-D slab geometry. *Earth and Planetary Science Letters*, 426:76–88.

Wada, I. and Wang, K. (2009). Common depth of slab-mantle decoupling: Reconciling diversity and uniformity of subduction zones. *Geochemistry Geophysics Geosystems*, 10(10):Q10009.

Wakabayashi, J. (2015). Anatomy of a subduction complex: architecture of the Franciscan Complex, California, at multiple length and time scales. *International Geology Review*, 57(February):37–41.

Wakabayashi, J. (2017). Structural context and variation of ocean plate stratigraphy , Franciscan Complex , California : insight into mélange origins and subduction-accretion processes. *Progress in Earth and Planetary Science*, 4:1–23.

Wakabayashi, J. and Dumitru, T. A. (2007). 40 Ar / 39 Ar Ages from Coherent , High-Pressure Metamorphic Rocks of the Franciscan Complex , California : Revisiting the Timing of Metamorphism of the World ' s Type Subduction Complex. *International Geology Review*, 49:873–906.

Whitney, D. L. and Hamilton, M. A. (2004). Timing of high-grade metamorphism in central Turkey and the assembly of Anatolia. *Journal of the Geological Society, London*, 161:823–828.

Zhao, D., Yanada, T., Hasegawa, A., Umino, N., and Wei, W. (2012). Imaging the subducting slabs and mantle upwelling under the Japan Islands. *Geophysical Journal International*, 190(2):816–828.

Solid Earth Discuss., https://doi.org/10.5194/se-2017-134
Manuscript under review for journal Solid Earth
Discussion started: 16 January 2018

Solid Earth Discussions
Open Access
EGU

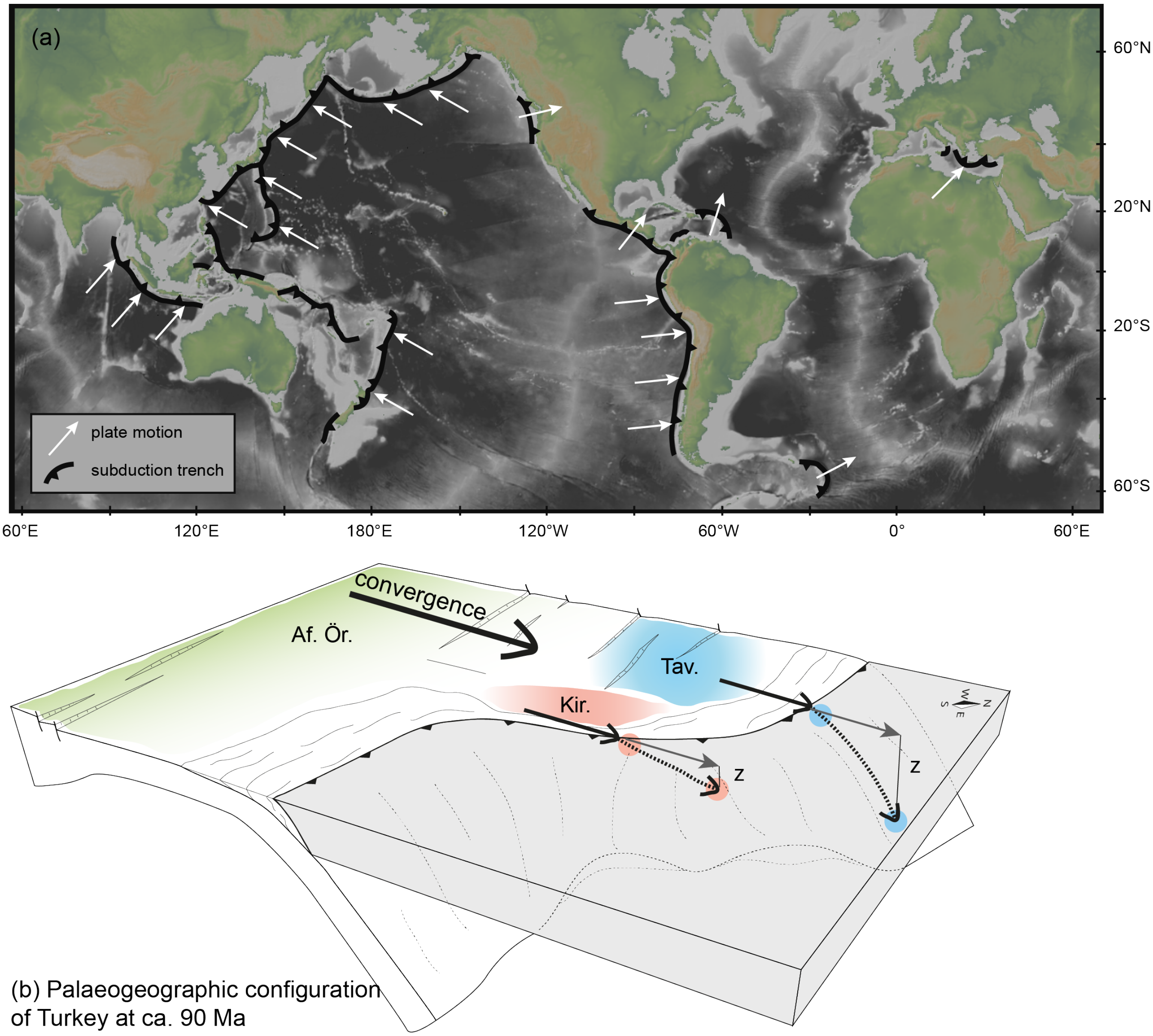

Figure 1. (a) Plate motion at trenches from the NNR-MORVEL model (Argus et al., 2011). Baselayer obtain with GeoMapApp (http://www.geomapapp.org) with topography and bathymetry from Ryan et al. (2009). Inset give the definition of parameters L_y and A used to characterize the geometry of the subduction zone. (b) Possible palaeogeographic configuration at *ca.* 90 Ma for Central Turkey based on the reconstruction of van Hinsbergen et al. (2016).

Solid Earth Discuss., https://doi.org/10.5194/se-2017-134
Manuscript under review for journal Solid Earth
Discussion started: 16 January 2018

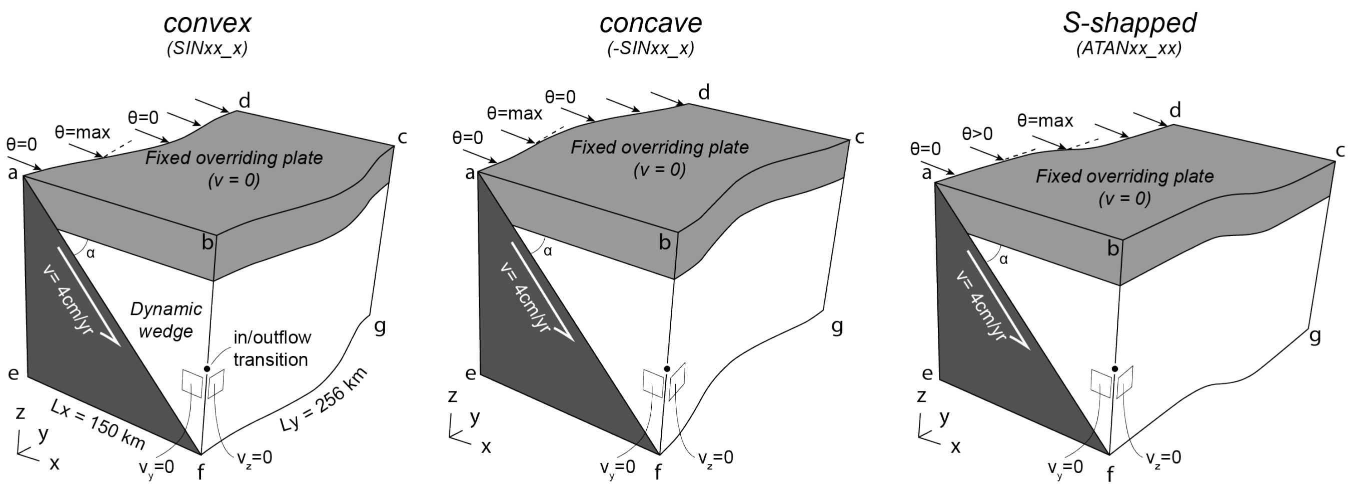

Figure 2. Setting of the computed models with the kinematic boundary condition. Initial thermal state is computed following the half-space cooling model following the formulation of Turcotte and Schubert (2014) with a 25 My old oceanic lithosphere for the downgoing slab and a 5 My old lithosphere for the upper plate.

Table 1. Physical parameter used in the numerical model

Symbol	Name	Value	Units
C_p	specific heat	1250	$J.kg^{-1}.K^{-1}$
ρ	volumetric mass density	3300	$kg.m^{-3}$
μ	effective viscosity	10^{22}	$Pa.s$
k	thermal conductivity	2.5	$W.m^{-1}.K^{-1}$

Solid Earth Discuss., https://doi.org/10.5194/se-2017-134
Manuscript under review for journal Solid Earth
Discussion started: 16 January 2018

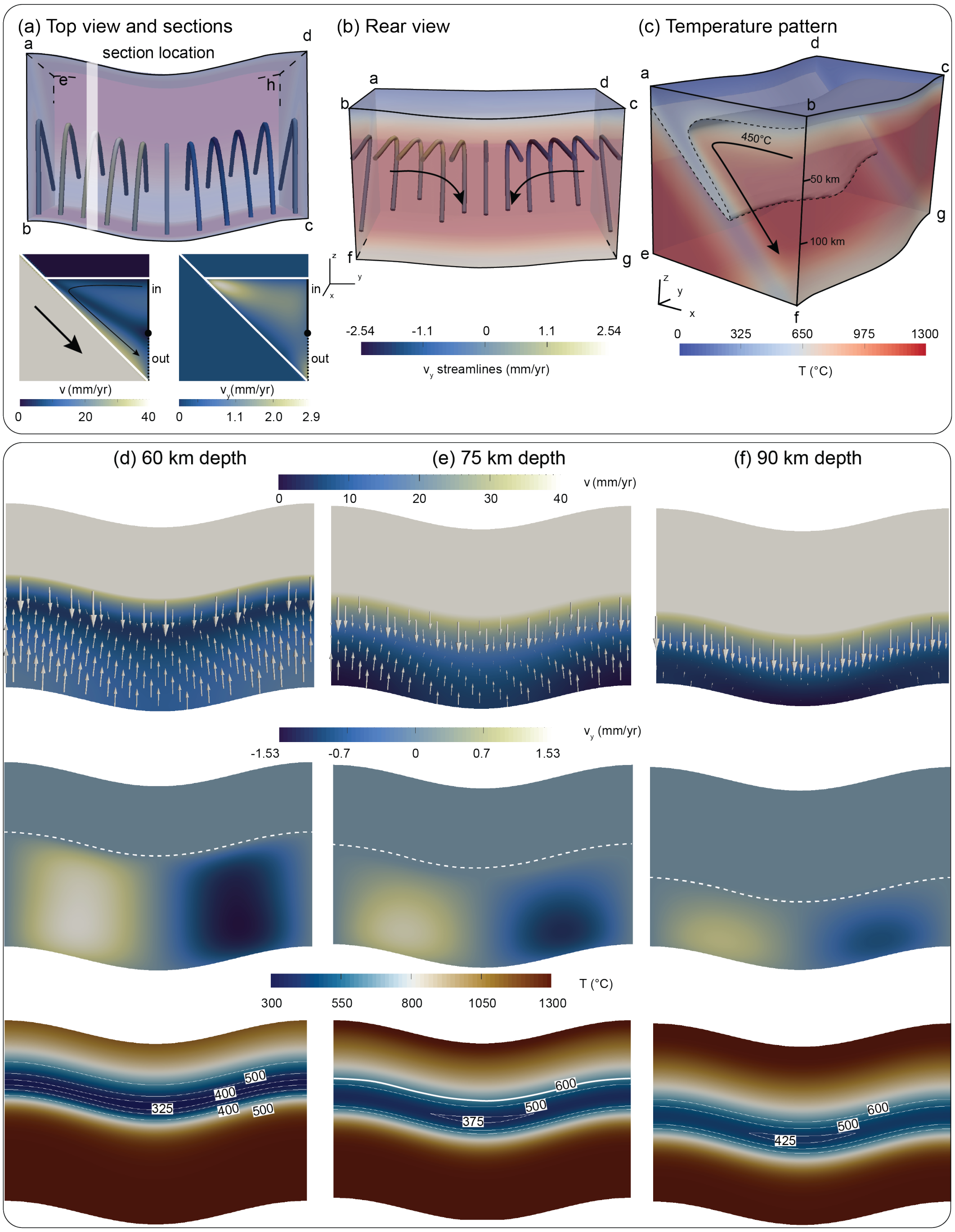

Figure 3. Results of the model SIN20_1. (a) Top view with streamlines showing the trench parallel mantle flow and sections $\boldsymbol{v}$ and v_y at $y = 64km$; (b) rear view of the domain with emphasis on the trench parallel flow represented as stramlines; (c) Temperature pattern in the model and deflection of the 450°C isotherm; (d) $\boldsymbol{v}$, v_y and T at 60 km depth; (e and f) same as (d) at 75 and 90 km depth.

Solid Earth Discuss., https://doi.org/10.5194/se-2017-134
Manuscript under review for journal Solid Earth
Discussion started: 16 January 2018

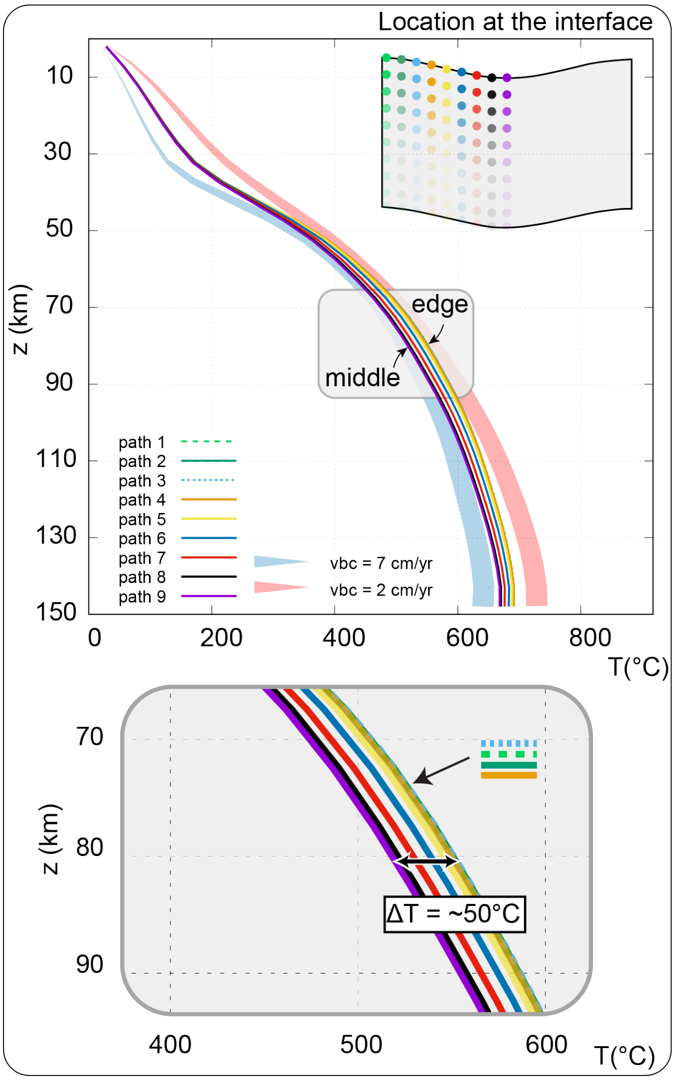

Figure 4. Depth–Temperature path at the plate interface of the reference model.

Solid Earth Discuss., https://doi.org/10.5194/se-2017-134
Manuscript under review for journal Solid Earth
Discussion started: 16 January 2018

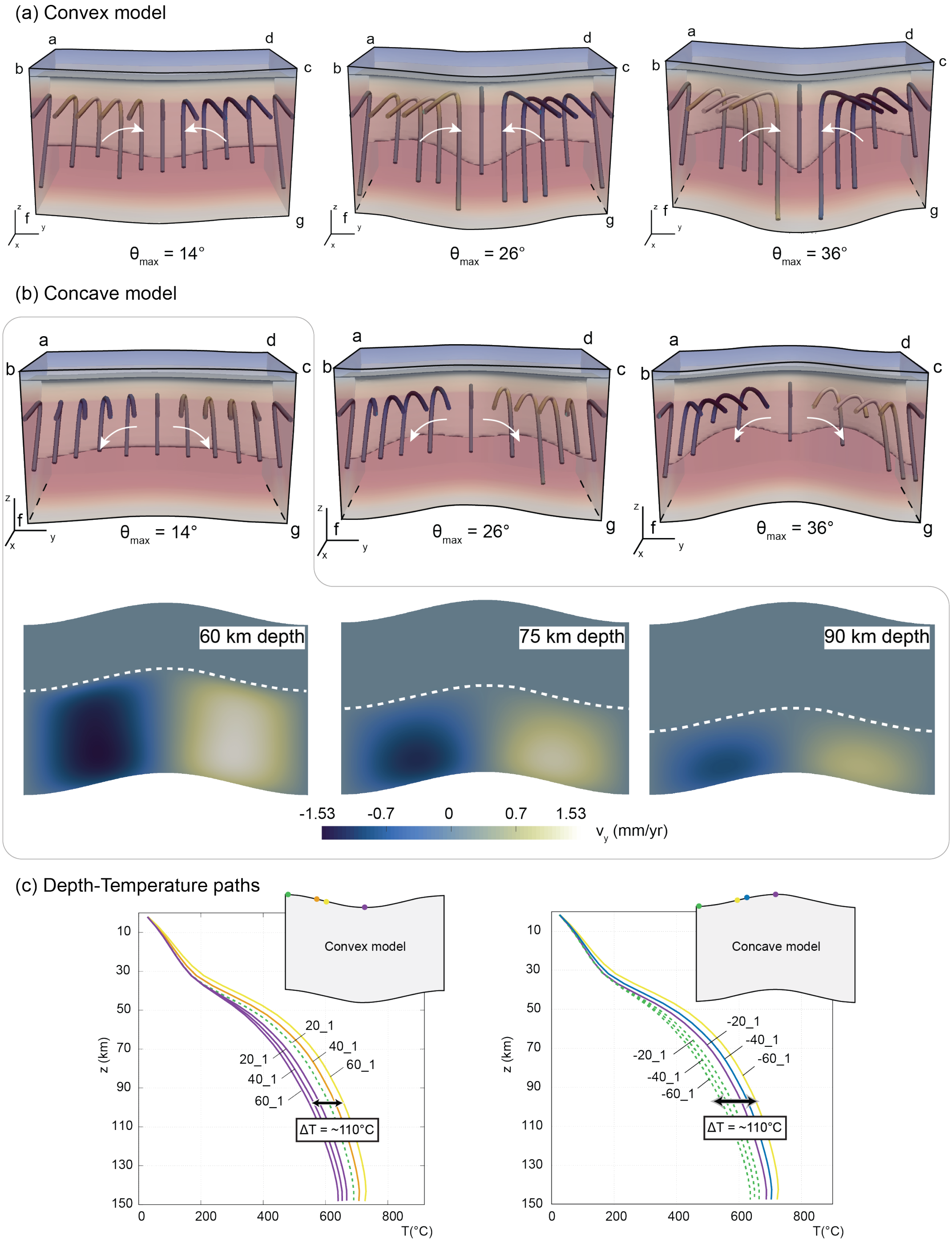

Figure 5. (a) Mantle flow, shape of the 450°C isotherm and depth temperature path for the convex models; (b) Mantle flow, shape of the 450°C isotherm and depth temperature path for the concave models

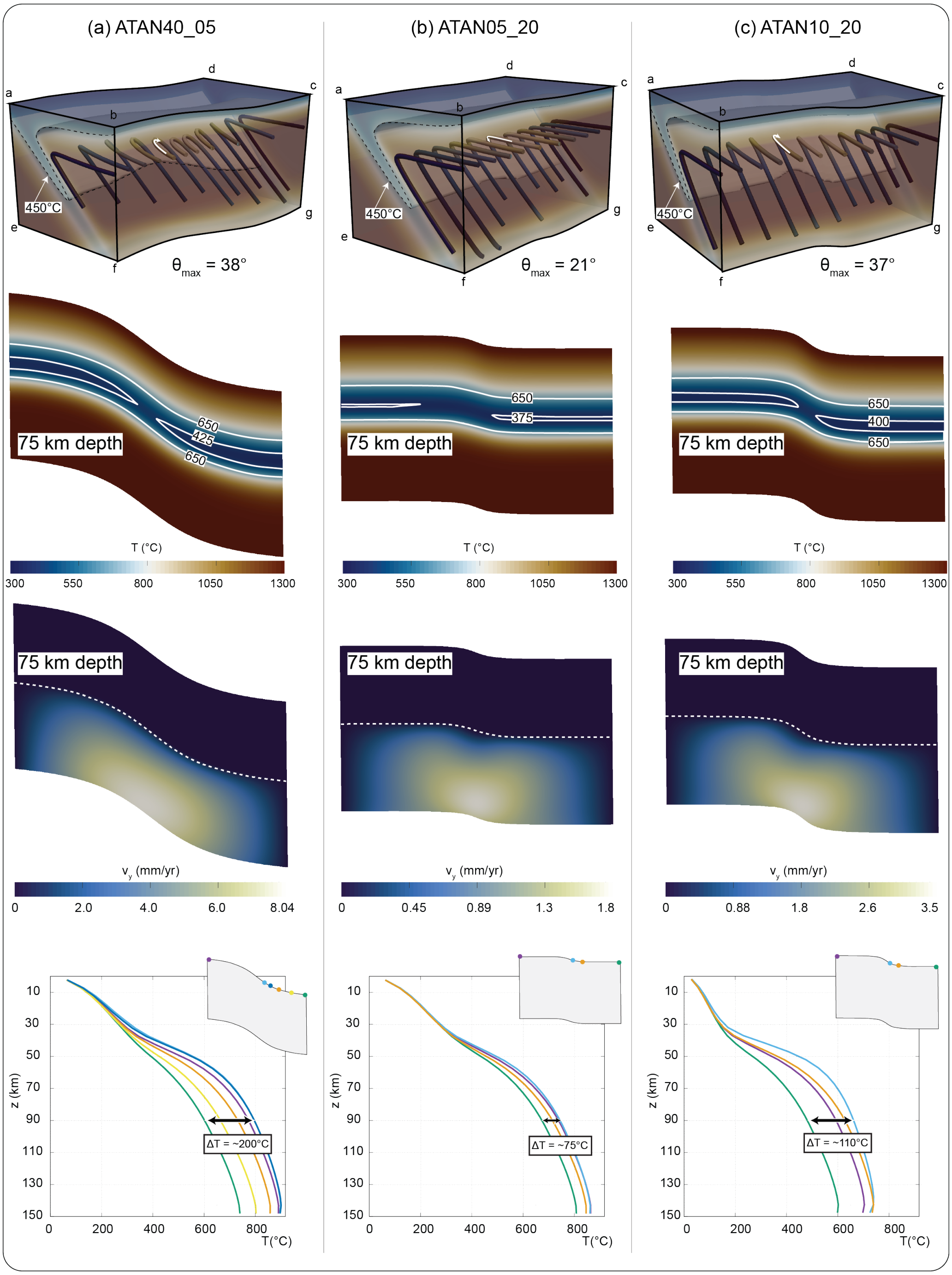

Figure 6. From to to bottom: 3D view of model ATANA_$\gamma\gamma$ showing the mantle flow streamlines and the contour of the 450°C isotherm and its more or less important deflection at the centre of the modeling space. Map of temperature at 75 km. Map of trench parallel velocity at 75 km depth. Depth–temperature path along the plate interface showing a ΔT of 200 °C with respect to the location in the model; (a) Model ATAN40_05; (b) Model ATAN05_20; (c) Model ATAN10_20

Solid Earth Discuss., https://doi.org/10.5194/se-2017-134
Manuscript under review for journal Solid Earth
Discussion started: 16 January 2018

Table 2. v_y in the mantle at different depth compared with the magnitude velocity at the same position

Model name		depth (km)	vel. (mm/yr) v_y	v	v_y/v
SIN20_1		60	1.54	13.2	12%
θ_{max}	14°	75	1.42	8.77	16%
$y_{\theta_{max}}$	±64	90	0.944	4.54	17%
SIN20_2		60	1.51	15.0	10%
θ_{max}	17°	75	1.28	10.5	12%
$y_{\theta_{max}}$	±42	90	0.976	4.13	24%
SIN40_1		60	3.08	10.4	23%
θ_{max}	26°	75	2.54	8.30	30%
$y_{\theta_{max}}$	±64	90	1.88	4.73	39%
SIN40_2		60	3.26	15.9	21%
θ_{max}	32°	75	2.76	11.0	25%
$y_{\theta_{max}}$	±42	90	2.14	3.79	56%
SIN60_1		60	4.68	12.3	38%
θ_{max}	36°	75	3.81	7.76	49%
$y_{\theta_{max}}$	±64	90	2.84	4.78	59%
SIN60_2		60	5.37	16.2	33%
θ_{max}	43°	75	4.58	10.9	42%
$y_{\theta_{max}}$	±42	90	3.59	3.67	98%